Digest Journal of Nanomaterials and Biostructures Vol. 20, No. 4, October-December 2025, p. 1675-1691

Optimization of cellulose extraction from pineapple crown waste and its application in capacitor composites

B. Sitorus [a,*], A. Antonius [a], B. Piluharto [b], S.D. Panjaitan [c]
[a] *Department of Chemistry, Universitas Tanjungpura, Pontianak, Indonesia*
[b] *Department of Chemistry, Universitas Jember, Jember, Indonesia*
[c] *Department of Electrical Engineering, Universitas Tanjungpura, Pontianak, Indonesia*

In this study, the optimization of cellulose extraction from pineapple crown waste and its application in capacitor composites were investigated. Extraction was conducted through delignification, bleaching, and sulfuric acid hydrolysis at 45, 50, and 55 °C, followed by ultrasonication. Characterization results showed that cellulose obtained at 50 °C, denoted as nanocellulose (NC)-50, exhibited particle sizes below 100 nm as determined by particle size analysis (PSA). Fourier transform infrared spectroscopy (FTIR) confirmed the effective removal of lignin and hemicellulose, while X-ray diffraction (XRD[1]) analysis revealed the highest crystallinity index for NC-50. To evaluate its functionality, NC-50 was composited with polypyrrole (PPy) and fabricated into a symmetric capacitor using parallel flat electrodes. Electrochemical measurements demonstrated a linear voltage–current (V–I) response, voltage-dependent capacitance (V–C), and stable charge–discharge behavior under operating voltages of 2–6 V. These results confirm that optimized cellulose from pineapple crown waste is a promising and sustainable matrix for capacitor composites in energy storage applications.

(Received September 29, 2025; Accepted December 31, 2025)

Keywords: Hydrolysis temperature, Nanocellulose, Pineapple crown, Polypyrolle

1. Introduction

Nanocellulose (NC), a cellulosic material with at least one particle diameter or width of 1-100 nm [1], has promising prospects in advanced material technology such as nanopaper, nanocomposite, drug delivery, adsorbent, renewable energy, and energy storage [2-5]. Researchers have tried to obtain NC from various sources, such as algae, bacteria, marine animals, or natural plant fibers [6-8]. Considered agricultural waste, pineapple crowns have become a feasible source for NC production, which unfortunately has not been widely applied [9]. Although many residues are generated in pineapple consumption as the crown is mostly discarded during consumption, few studies have been conducted regarding using pineapple crowns as a source of NC. The pineapple crown accounts for approximately 10% to 25% of a pineapple's total weight. With a cellulose content of about 85%, hemicellulose of 7%, and lignin of 5%, the crown is suitable for getting cellulose [9, 10].

Two main types of NC are distinguished: crystalline NC (CNC) and cellulose nanofibrils (CNF). CNC refers to NC obtained via acid hydrolysis under controlled thermal and temporal conditions [1], whereas CNF is mainly produced by mechanical disintegration [11]. The process of producing CNC, including pretreatments and variation in hydrolysis stages of the material, is related to the characteristics of the obtained CNC particle size [11, 12]. One of the most significant current discussions in obtaining CNC from lignocellulosic material is getting the best conditions in the hydrolysis process, mainly regarding the acid type and concentration used to hydrolyze the material.

* Corresponding author: berlian.sitorus@chemistry.untan.ac.id
https://doi.org/10.15251/DJNB.2025.204.1675

Various acids, including H_2SO_4, HCl, and CH_2O_2 have been used in the hydrolysis process [10, 12-13]. A hydrolysis process utilizing orange juice and ball milling has been carried out [14] while producing CNF from pineapple leaf fibers, as they tried to use an environmentally friendly acid. However, the obtained cellulose diameter was still in the microsize range of 3.27-4.78 μm. The three-hour ball milling process reduced the cellulose diameter to 48.5-51.7 nm, increasing its crystallinity by 20%. H_2SO_4 is commonly employed as it introduces sulfate groups onto the cellulose surface, imparting negative charges that enhance colloidal stability in aqueous suspension [15]. The work in [10] converted pineapple crown leaves into CNC by hydrolysis using 60% H_2SO_4 at 45 °C. The obtained CNC displayed a whisker-like (needle-shaped) morphology, averaging 39 ± 12 nm in diameter, a mean longitudinal dimension of 245 ± 110 nm, with a crystallinity level reaching 73%.

Another study has also synthesized CNC from pineapple crown fibers using H_2SO_4 at 50°C with acid concentrations of 50 and 64%, and hydrolysis time variations of 60- and 120-minute. Hydrolysis using 64% sulfuric acid for two hours yielded the best results: a NC size of 140 nm, zeta (z) potential -47.69 mV, and a crystallinity index of 87.44% [12]. Most studies have emphasized optimizing hydrolysis parameters, such as acid concentration and reaction time, to achieve NC with desirable properties such as small particle size, high crystallinity, and good colloidal stability [1, 2]. However, limited research has thoroughly investigated how hydrolysis temperature affects the properties and performance of NC obtained from pineapple crown biomass. While optimizing extraction remains critical, NC has also gained attention for its role in energy applications. Though not inherently redox-active, NC porous structure, hydrophilicity, and mechanical strength make it an excellent scaffold for redox-active polymers like polypyrrole (PPy), supporting ion transport and structural integrity [3, 4].

Recent advances in supercapacitor development have reported well-designed hierarchical carbon superstructures with high surface area and efficient ion diffusion channels, enabling exceptional energy and cycling performance in zinc-ion hybrid capacitors [16, 17]. These works highlight the rapid progress of high-energy supercapacitor research and provide context for exploring sustainable electrode materials, such as NC-based composites. This study extracted NC from pineapple crown under varying hydrolysis temperatures. The sample exhibiting the most favorable characteristics was subsequently composited with PPy and fabricated into a parallel-plate capacitor. Electric parameter measurements were employed to assess the electrochemical response and validate its charge storage behavior. This approach evaluates the suitability of pineapple-derived NC as an energy material component and highlights a sustainable pathway for valorizing agricultural residues in advanced material applications.

2. Experimental methods

The experimental work utilized the following materials: distilled water, 95-97% ethanol, ice cubes, and filter paper. Pineapple crowns were collected from a local market in Pontianak City, Indonesia, and served as the main cellulose starting material. The reagents comprised sulfuric acid (H_2SO_4) for acid hydrolysis, NaOH and NaOCl (12%, technical grade) for bleaching, and $NaHCO_3$ for pH adjustment. Commercial cellulose (CC) was used as a reference material for comparative characterization. Pyrrole, Ferric chloride ($FeCl_3$), and Polyvinyl alcohol (PVA) were incorporated into the cellulose matrix to form a composite material, enabling evaluation of electrochemical properties. All analytical-grade chemicals, unless otherwise stated, were obtained from Merck. The methodology comprises three main stages: preparation of NC from pineapple crown biomass via chemical pretreatments and acid hydrolysis; physicochemical characterization of NC; and fabrication of NC–PPy composite electrodes, followed by electrochemical analysis to evaluate their charge storage performance.

2.1 Extraction of NC from pineapple crown biomass

Figure 1 illustrates the stepwise procedure for obtaining NC from pineapple crown biomass. The process involved delignification and bleaching of Pineapple Crown Powder (PCP) to yield Cellulose After Bleaching (CAB), followed by sulfuric acid hydrolysis and ultrasonication to obtain NC (Figure 1(f)). Then, a series of characterizations was performed to evaluate the physicochemical

transformation at each stage. The raw pineapple crown waste was collected from traditional markets in Pontianak, West Kalimantan, Indonesia (Figure 1(a)). The crown was manually peeled, cleaned (Figure 1(b)), and chopped into 5 mm × 1 cm fragments. These pieces were sun-dried for 3–5 days (Figure 1(c)), followed by grinding and sieving through a 200-mesh screen to obtain PCP, as shown in Figure 1(d).

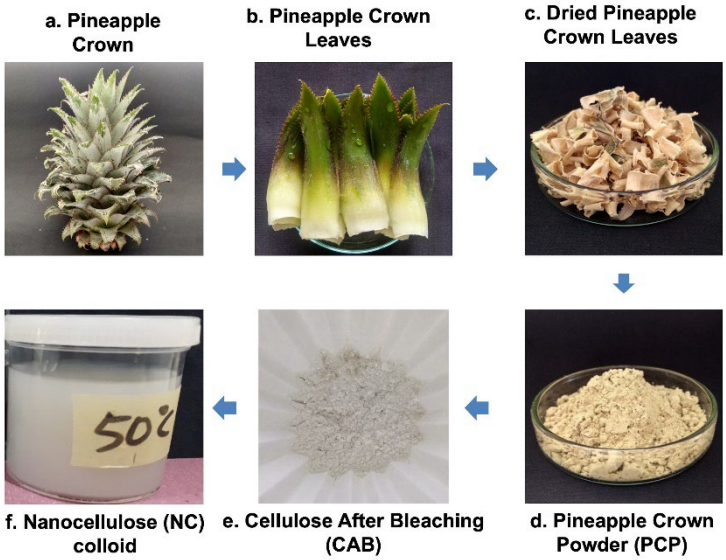

Fig. 1. The stages and outcomes in nanocellulose (NC) extraction derived from the pineapple crown biomass.

The process consisted of stirring PCP in 10% NaOH at a 1:10 (w/v) solid-to-liquid ratio, maintained at 80 °C and 400 rpm for 1 hour to break down the lignin–cellulose matrix. Filtration and subsequent washing continued until it reached a near-neutral pH. Bleaching was followed in a 7% NaOCl solution was applied at a 1:20 (w/v) ratio, the mixture was maintained at a constant temperature of 50 °C and agitated at 200 rpm for a duration of two hours.

This process produced a cellulose-enriched material, labeled CAB and illustrated in Figure 1(e). The cellulose yield corresponding to this stage was calculated using (1)

$$\text{Yield (\%)} = \left({}^{W_1}/_{W_2}\right) \times 100 \quad (1)$$

Where W1 and W2 are the CAB and PCP mass, respectively.

To produce NC from CAB, the material underwent hydrolysis in 40% H_2SO_4 solution (1:20 w/v) for 2 hours at 45, 50, and 55 °C, then was promptly quenched by introducing cold distilled water in a 1:5 ratio. The resulting suspension was then homogenized and spun at 3000 rpm over a 100-minute duration, followed by thorough washing of the precipitate with cold distilled water, and subsequently neutralized with 0.5 M $NaHCO_3$ to adjust the supernatant pH to 7.0–7.5. Ultrasonication at 20 kHz for 10 minutes was applied to the final suspension using a Branson Sonifier 250 to produce NC, as illustrated in Figure 1(f). Samples were designated as NC-45, NC-50, and NC-55, corresponding to hydrolysis temperatures of 45, 50, and 55 °C, respectively. Each colloid was heated at 105 °C to achieve a constant mass.

2.2 Characterizations of NC

Fourier Transform Infrared (FT-IR) spectroscopy was performed using a Shimadzu IR Prestige-21 to identify functional groups in PCP, CAB, and NC, with spectra acquired in the 4000–600 cm^{-1} range. The crystallinity of PCP, CAB, and NC was analyzed using an X-ray diffractometer

(XRD). The XRD type that has been used was D8 Advance from Bruker. XRD was conducted using a source emitting at 1.54060 Å, under operating conditions of 40 kV, and 40 mA, with a rotation rate of 5000°/min. Radiation intensity was recorded over the 2θ range of 5° to 100°. Crystallinity indices were determined by deconvoluting the XRD diffractograms using Origin 2018 software and calculated using (3), where CI represents the crystallinity index (%), Ac represents crystalline peak area, whereas Aa corresponds to the amorphous region.

$$CI\ (\%) = \frac{A_c}{A_c + A_a} \times 100 \quad (3)$$

We employed a Particle Size Analyzer to examine the particle size distribution and ζ-potential of the NC-45, NC-50, and NC-55 suspensions. The analysis used a Malvern Zetasizer v7.01, covering a size range of 0.1–10,000 nm. Each sample underwent five repeated measurements to determine the average values.

2.3 Composite formation and electrode preparation

PPy/cellulose composites were synthesized via in situ polymerization, adapting a previously reported method for conducting polymer composites [18]. To initiate the process, 0.3 g of the optimally extracted cellulose was suspended in 80 mL distilled water along with 1.5 mL of pyrrole monomer. The suspension was then sonicated for one hour to ensure uniform dispersion. $FeCl_3$ solution was introduced dropwise as the oxidizing agent, and the polymerization was conducted at room temperature for over 4 hours. The resulting composites were collected and prepared for electrode fabrication. Aluminum sheets (3 × 3 cm) were pretreated in 1 M NaOH solution and dried. To form the electrode gel, PPy/cellulose composites were blended with PVA previously dissolved at 40 °C, and the mixture was uniformly applied to the aluminum substrates, followed by ambient drying. Graphite electrodes were prepared following the same procedure, substituting the composite with graphite powder.

3. Results and discussions

3.1 Cellulose extraction from pineapple crown into NC

The CAB yield obtained from PCP was 14.11 ± 0.607% using (1). The amount is similar to other research results [14], which got 11.0 ± 4.0% cellulose yield from pineapple crown. This similarity supports the reproducibility and reliability of the extraction procedure for recovering cellulose from agricultural waste sources. Hydrolysis was done to remove the amorphous cellulose part to increase the crystallinity. As reported [19], hydrolyzing pineapple crown cellulose with 40% H_2SO_4 produced the most favorable visual and structural quality result. The sample appeared noticeably whiter and brighter than those treated with 30% and 60% H_2SO_4, which yielded yellowish and blackened residues, respectively. The lower acid concentration (30%) was insufficient for complete hydrolysis, while the higher concentration (60%) likely caused excessive degradation of cellulose into glucose, leading to carbonization. In contrast, the treatment with 40% acid enabled efficient breakdown of the fibrous matrix, yielding a well-bleached suspension with minimal by-product formation. The remaining H_2SO_4, sugar, and dissolved salts in the cellulose suspension were separated by centrifugation, leaving the cellulose in the precipitate [12, 19]. To neutralize residual H_2SO_4 in the cellulose, we introduced $NaHCO_3$ into the washing water, allowing it to react as follows [20]:

$$2NaHCO_{3\,(aq)} + H_2SO_{4\,(aq)} \rightarrow Na_2SO_{4(aq)} + 2H_2CO_{3(aq)}$$

Three different hydrolysis temperatures were employed in this study to determine the optimal conditions for producing NC with superior characteristics, particularly in terms of particle size and crystallinity index. Hydrolysis temperature significantly influences cellulose degradation behavior. Very high temperatures may lead to over-hydrolysis, resulting in cellulose degradation into glucose, often indicated by a dark brown discoloration of the sample [21]. On the contrary, low temperatures may not effectively eliminate amorphous regions, yielding cellulose with lower

crystallinity. Therefore, evaluating multiple temperature points is essential to balance effective hydrolysis and structural preservation.

Ultrasonication was employed to disperse NC and inhibit its agglomeration [22], as the ultrasonic waves generate acoustic energy capable of inducing cavitation. This process generates gas bubbles that implode at high speed, applying mechanical force to disrupt hydrogen bonding within the cellulose matrix [23, 24]. When applied at sufficient intensity, this energy also facilitates the diffusion of dissociated H^+ ions from H_2SO_4 into the cellulose matrix, thereby degrading its amorphous regions [25].

As presented in Table 1, the NC obtained from hydrolysis at 55 °C exhibited the lowest average solids content, followed by samples prepared at 50 °C and 45 °C. This trend qualitatively indicates that NC-55 contains the smallest amount of dispersed NC particles among the three. The reduced solids content in NC-55 suggests that partial degradation of cellulose into glucose may have occurred at this higher temperature. Furthermore, the lower solids content in NC-50 compared to NC-45 suggests a more extensive degradation of the non-crystalline zones within the cellulose matrix, contributing to a reduced yield of solid NC.

Table 1. Average solids content of NC at various hydrolysis temperatures.

Notation	Hydrolysis Temperature (°C)	Average Solids Content (%)
NC-45	45	2.040
NC-50	50	1.930
NC-55	55	0.665

3.2 FT-IR spectral analysis

The PCP spectrum showed general peaks of lignocellulose composed of cellulose, hemicellulose, and lignin. A distinct peak at 1431.2 cm^{-1} confirms the presence of cellulose in PCP [26]. Stretching vibrations of hydroxyl (O–H) groups, associated with intra- and intermolecular hydrogen bonding, were observed between 3270–3418 cm^{-1} [10, 12, 24, 26-28]. The symmetric and asymmetric C–H stretching from CH_2 groups appear at 2901–2922 cm^{-1}. The broadband at 1631–1641 cm^{-1} corresponds to O–H bending of water absorbed by cellulose [10, 12, 24, 26-28]. Glycosidic C–O–C stretching vibrations, typical of the bonds linking glucose units, are detected at 894–897 cm^{-1} [12, 18, 24, 27]. A characteristic lignin peak appears near 1602 cm^{-1}, corresponding to phenolic and conjugated C–H stretching in aromatic rings [21]. Another lignin-related signal at ~1251 cm^{-1} is attributed to syringyl ring vibrations [8]. The peak around 1730 cm^{-1} indicates C=O stretching of uronic acids from hemicellulose, which may also originate from acetyl ester groups or ester linkages between cellulose, hemicellulose, and lignin [10, 12, 26-28].

The CAB spectrum in Figure 2 shows the absence of peaks at 1251, 1602, and 1730 cm^{-1}, indicating successful removal of lignin and hemicellulose through pretreatment and bleaching. New peaks emerging at 1053–1059, 1095–1105, and 1369–1390 cm^{-1} confirm the presence of cellulose, corresponding to C–O–C stretching of pyranose rings [27], symmetric stretching of glycosidic bonds [21], and pyranose skeletal vibrations [27], respectively.

Compared to PCP, CAB also exhibits stronger peak intensities, suggesting a higher cellulose content. These results demonstrate that the pretreatment and bleaching steps effectively purified cellulose from pineapple crown waste, making CAB a suitable precursor for NC synthesis. Subsequent hydrolysis with sulfuric acid introduced new absorption bands at 606–611 and ~845 cm^{-1}, corresponding to C–O–S symmetric stretching of sulfate hemiesters [29, 30]. Additional peaks at ~952 and 1278–1279 cm^{-1} are associated with S–O and asymmetric S=O stretching, indicating sulfate groups attached to the cellulose surface [31, 32]. Bands at 1426–1428 cm^{-1} are associated with crystalline cellulose, while the ~1549 cm^{-1} peak corresponds to aldehydic C=O stretching, indicating cellulose degradation into glucose [33].

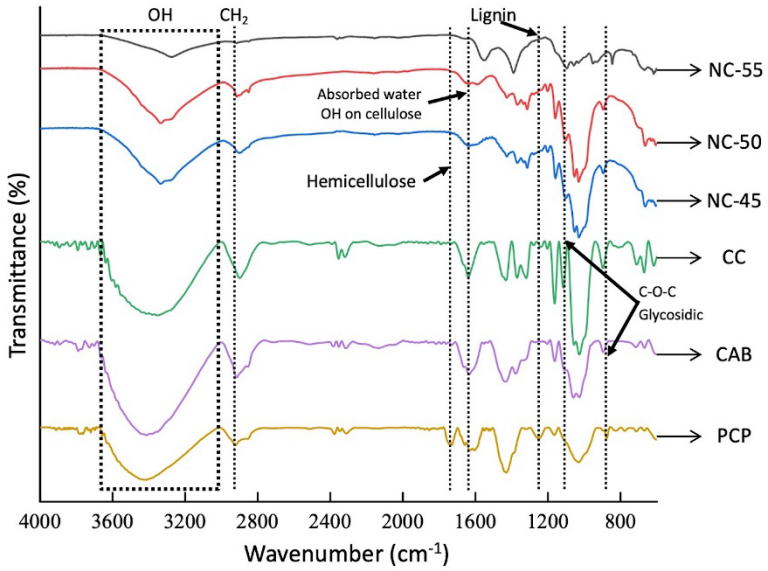

Fig. 2. FT-IR spectra of pineapple crown powder (PCP), cellulose after bleaching (CAB), commercial cellulose (CC), NC-45, NC-50, and NC-55.

As shown in the NC-45 spectrum, new peaks appear at 1279 and 1427 cm^{-1}, indicating that hydrolysis and ultrasonication successfully enhanced cellulose crystallinity. However, the absence of peaks around 606–611, ~845, and ~952 cm^{-1} suggests minimal sulfate group presence, implying incomplete hydrolysis at 45 °C. The lack of a ~1549 cm^{-1} peak confirms that cellulose was not broken into glucose [19, 25]. The NC-50 spectrum displays new peaks at 606.8, 1279.3, and 1427.5 cm^{-1}, indicating that hydrolysis and ultrasonication successfully increased cellulose crystallinity. The distinct 606.8 cm^{-1} peak suggests the presence of sulphate groups, confirming that hydrolysis at 50 °C was effective. Meanwhile, the absence of a ~1549 cm^{-1} peak indicates that cellulose was not converted into glucose [34, 35]. In the NC-55 spectrum, peaks appear at 611, 846, 952, and 1549 cm^{-1}, suggesting hydrolysis at 55 °C led to cellulose decomposition into glucose. The absence of peaks at 894–897 and 1158–1165 cm^{-1} further supports the cleavage of glycosidic bonds. This degradation reduces the crystalline structure of cellulose, as indicated by the missing 1426–1428 cm^{-1} peaks [20, 24].

3.3 XRD analysis

All peaks that appear on the diffractogram indicate the crystalline portion of cellulose. In contrast, the amorphous portion has the lowest intensity at around 18° in Figure 3. The cellulose diffraction pattern obtained has the highest intensity peak at $2\theta \approx 22°$ with a double peak at 15 and 16° and another peak at 34°. Each of these peaks has a Miller index (200) for 22-22.5°, while ($11\bar{0}$), (110), and (004) are owned by 15, 16, and 34°, respectively. All the peaks were characteristic of the type I cellulose structure with semicrystalline properties [36-40]. Cellulose type I is a crystalline biopolymer composed of two natural allomorphs: Iα (triclinic) and Iβ (monoclinic) [1], [39]. Cellulose Iα can only be found in lower plants, such as bacterial and algal cellulose, while cellulose Iα comes from higher plants with cell walls, such as pineapple [40].

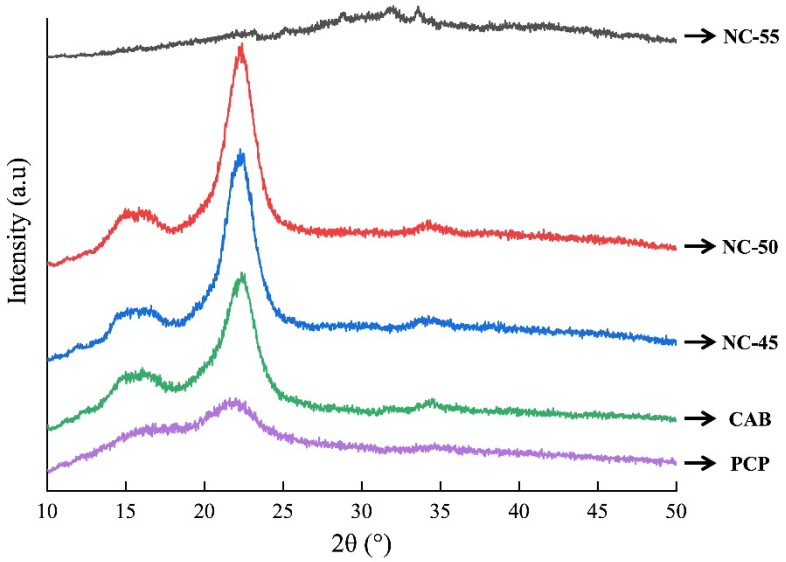

Fig. 3. X-ray diffraction profiles of PCP, CAB, NC-45, NC-50, and NC-55.

The increase in the crystallinity index in CAB (Table 2) indicates the loss of hemicellulose and lignin components, which FT-IR spectra have proved in the previous discussion. In addition, the appearance of a $2\theta \approx 34°$ peak, which is more pronounced in the CAB diffractogram than PCP, indicated an increase in the crystallinity of cellulose. Pineapple crown and cellulose extracted in this study had a lower crystallinity index than in the literature. Other research has a pineapple crown crystallinity index of 39.6% and cellulose of 43.05% [14]. Variations in crystallinity index are influenced by residual hemicellulose and lignin content. Additionally, the presence of amorphous parts in cellulose is a factor causing the small CAB crystallinity index. Elimination of amorphous domains enhanced crystallinity and resulted in smaller CNC crystallites. Hydrolysis of cellulose at a temperature of 45°C has increased the crystallinity index by 8.5% compared to CAB. This shows that the amorphous portion of cellulose has been reduced, and its rigidity has increased. Hydrolysis at 50 °C led to a 15.7% increase in cellulose crystallinity relative to CAB.

Table 2. Crystallinity index of pineapple crown-derived samples at various processing stages.

Notation	Crystallinity Index (%)	Crystal Size (nm)
PCP	19.8	33.2
CAB	34.4	14.7
NC-45	42.9	8.9
NC-50	50.1	3.3
NC-55	4.6	11.6

However, the crystallinity of cellulose decreased to 4.6% when hydrolysis was carried out at 55°C compared to CAB. As a result, the NC-50 diffraction pattern has a narrower peak than CAB, NC-45, and NC-55. The decrease in the crystallinity index was caused by H_2SO_4 attacking the crystalline part of cellulose because the amorphous part had been lost [8]. In this research, the most effective hydrolysis temperature for increasing the crystallinity of cellulose is 50°C. Similar

diffraction positions have also been reported in the literature for bacterial cellulose, although when PPy was incorporated into the cellulose framework, the intensity of these peaks was reduced and a broad amorphous background around 20–25° appeared due to the presence of PPy [41]. A comparable broad amorphous contribution of PPy is also visible in the XRD patterns of other PPy-based composites, such as PPy@V_2O_5@C, where the PPy phase contributes a diffuse peak in the same 20–25° region [42]. These comparisons confirm that while the fundamental diffraction angles remain consistent with cellulose I, the absence of PPy in our sample results in sharper and more defined peaks, highlighting the unmodified crystalline structure of the cellulose.

3.4 Particle size analysis and ζ-potential measurements

To evaluate the effect of hydrolysis temperature on particle size, all measurements were conducted in five replicates and summarized using mean values with standard deviations (mean ± SD). The analysis prioritized the number-based size distributions, as these more accurately reflect the actual particle population in suspension. The small particle size indicates the stability of the NC suspension in water. This stability arises from the substitution of hydroxyl groups with negatively charged sulfate ions, enhancing electrostatic repulsion [23]. Table 3 indicates that NC-45 has the smallest average particle size, suggesting superior colloidal stability relative to NC-50 and NC-55.

Table 3. Particle size distribution, Z-average and ζ-potential of NC with variations in hydrolysis temperature.

NC sample	Particle Size (nm)	Z-Average (nm)	ζ-Potential (mV)
NC-45	19.5 ± 4.3	571.2 ± 0.8	-25 ± 1.4
NC-50	25.9 ± 5.6	860.7 ± 0.9	-15 ± 0.9
NC-55	81.8 ± 20.6	583.2 ± 0.9	-34 ± 1.1

At 45°C and 50°C, the number-based PSA consistently fell within the 9 to 26 nm range, with low variation across replicates. Even at 55°C, although the average particle size increased, the values largely remained within the sub-100 nm scale. According to widely accepted definitions, a material is considered nanoscale if at least one of its dimensions is below 100 nm. On this basis, the NC produced in all three conditions satisfies the criteria for nanomaterials.

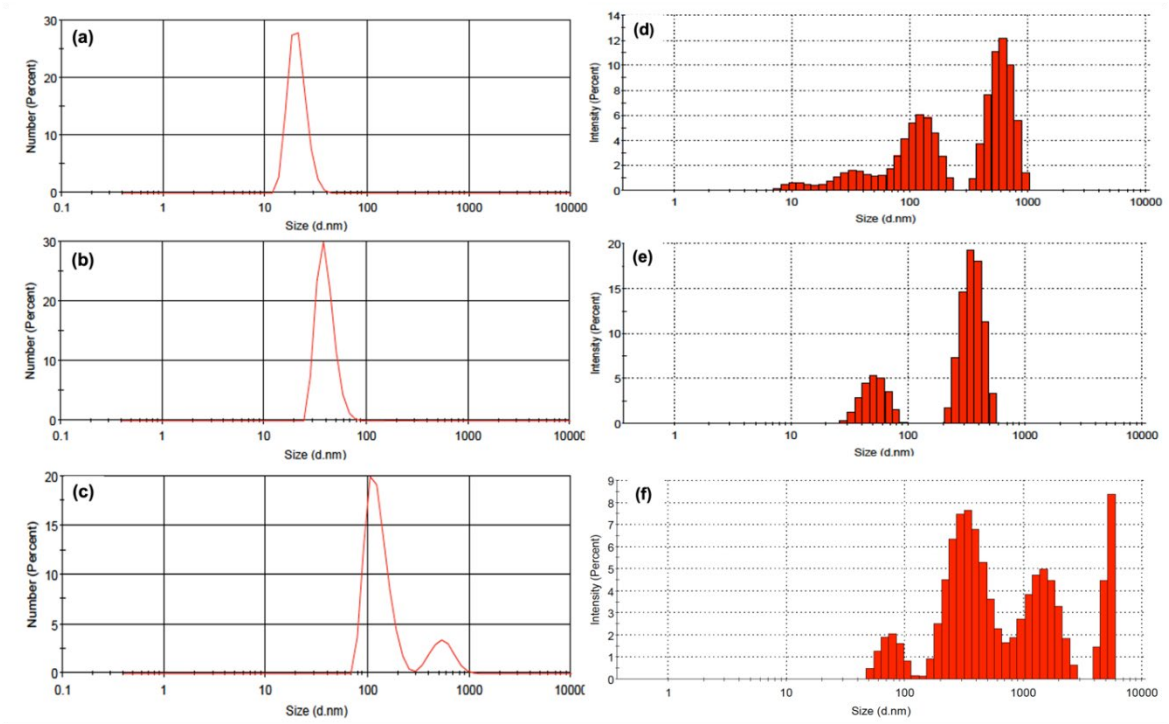

Fig. 4. Representative particle size distribution of the extracted NC by number (a–c) and Z-average intensity (d–f): (a, d) for NC-45; (b, e) for NC-50; and (c, f) for NC-5.

Figure 4 shows selected examples of particle size distribution for NC-45, NC-50, and NC-55. Charts (a–c) represent the size distribution by number, while (d–f) show distributions by intensity, reflecting Z-average values better. The samples are ordered as follows: NC-45 in (a) and (d), NC-50 in (b) and (e), and NC-55 in (c) and (f). Each plot was taken from one of five replicate measurements and is included here to give a visual sense of the data trends. The complete set of averaged values and statistical analysis can be found in Table 3, which forms the basis for the conclusions drawn.

The Z-average was relatively high (570–860 nm), which is expected due to the influence of occasional large aggregates in intensity-weighted DLS measurements. Such aggregation may result from strong non-covalent hydrogen linkages among molecular chains and Van der Waals forces between NC particles [43]. Despite this, the overall dispersion remained in the nanoscale range. The PdI ranged between 0.74 and 0.92, indicating a broad yet typical size distribution for lignocellulosic systems. Importantly, these values were consistent across all replicates, reflecting a stable and reproducible dispersion. Overall, the dominance of nanoscale particles in number-based data and the stable PdI confirm the effectiveness of the hydrolysis method in producing NC from pineapple crown waste.

The negative charge on NC can be seen from the ζ-potential, smaller than zero. The greater the negative charge, the bigger the repulsion between NC particles because of the electrostatic forces, so they are well dispersed [10]. NC is said to be well dispersed if ζ-potential > -25 mV and no aggregation occurs at ζ--potential > -15 mV [12, 22, 44].

The ζ-potential presented in Table 3 indicates the colloidal stability of the NC suspensions and reflects on the composites' electrochemical performance, particularly in pseudocapacitive systems. NC-55, with the most negative ζ-potential (–34 mV), suggests strong repulsion between NC particles, resulting in a well-dispersed suspension. This dispersion promotes better contact between the PPy matrix and electrolyte ions, potentially enhancing redox activity due to improved ion accessibility. However, the larger particle size of NC-55 may limit surface area interaction, which could reduce effective capacitance.

In contrast, NC-50, despite showing less colloidal stability (–15 mV), demonstrates the highest Z-average, which may arise from partial aggregation. Nevertheless, this sample offers a balanced structural framework, where sufficient hydroxyl functionality facilitates interaction with PPy, enhancing charge transport [45]. Such characteristics may account for the favorable electrochemical behavior observed in charge–discharge measurements, positioning NC-50 as an optimal candidate for capacitive applications under moderate voltages.

Thus, while high ζ-potential supports dispersion, its influence on capacitive properties must be considered alongside particle size, morphology, and polymer interaction. Combining electrostatic stability and conductive integration appears critical for achieving optimal capacitance performance in cellulose–PPy composites. The results confirm that CNC can be successfully produced from pineapple crown waste through acid hydrolysis, with 45 °C and 50 °C yielding the most favorable outcomes. Among them, NC-50 displays an effective balance of particle size, crystallinity, and surface charge, making it suitable for optimizing material performance in various applications, including capacitor applications. These findings underscore the importance of hydrolysis temperature in tuning CNC's size distribution and structural properties for targeted material performance.

3.5 Analysis of PPy/cellulose composites for electrochemical performance

This work explores the use of pineapple crown-derived NC in capacitive composite materials. We integrated the cellulose with PPy to fabricate a parallel plate capacitor. Then, we analyzed its electrochemical behavior through three key measurements: the voltage–current (V–I) characteristics, the voltage–capacitance (V–C) relationship, and the time-dependent charging–discharging response. The capacitive performance of the NC–PPy composite, formulated using NC hydrolyzed at 50 °C (NC-50), was evaluated under varying input voltages from 2 to 6 V.

Figure 5 compares the current response of PPy composites containing extracted and CC across a 2–6 V range. Both materials display increasing current with voltage, confirming their conductive nature. The PPy/CC composite exhibits a more linear and higher current output, suggesting improved charge transport, likely due to better polymer dispersion or interfacial contact. Meanwhile, the extracted cellulose sample maintains conductivity but shows slight deviations at higher voltages, possibly influenced by structural variations in the cellulose network. The improved conductivity observed in the PPy/cellulose composites is particularly relevant for electrochemical applications, where efficient electron transfer is essential [46]. This property is influenced by the presence of PPy and how it is distributed within the cellulose matrix. In this study, the more linear current response of the CC composite may reflect better polymer dispersion and interfacial contact. A similar observation was made by [47], who linked uniform PPy distribution to enhanced charge mobility and lower resistance, contributing to superior device performance. We evaluated the capacitive performance of the composites by analyzing their V–C curves (Figure 6), following the electrical conductivity measurements presented in Figure 5.

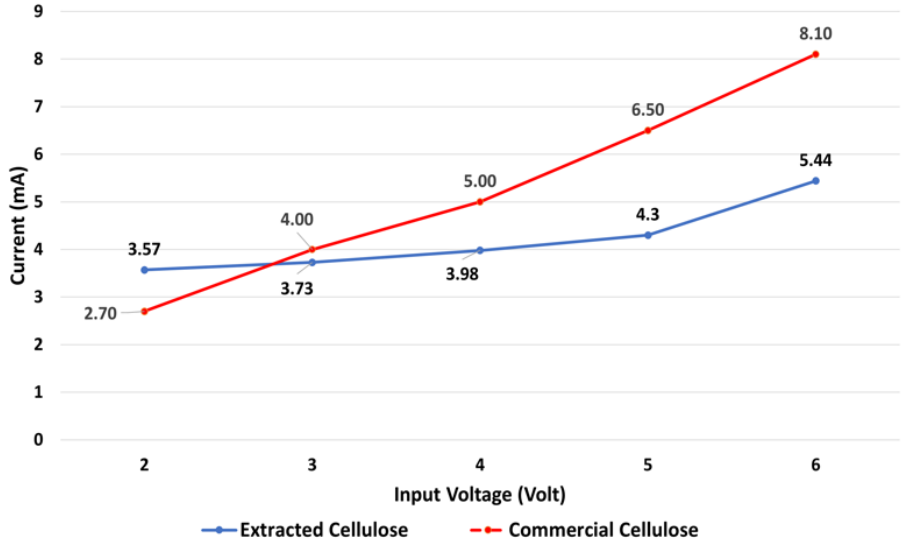

Fig. 5. V–I curve of extracted cellulose and CC composites showing current response under increasing input voltage.

The V–C curves of the two composites shown in Figure 6 exhibit distinct profiles: the extracted cellulose composite forms a gently declining slope, whereas the CC curve remains relatively flat, highlighting their different responses to the applied voltage. The extracted cellulose composite shows a higher initial capacitance of 5.68 µF at 2 V, gradually decreasing to 2.89 µF at 6 V. This trend may reflect intense polarization at low voltages and a dynamic dielectric response under increasing electric field. In contrast, the CC composite displays a capacitance profile across the voltage range, varying between 3.96 µF and 4.30 µF, indicating consistent dielectric performance. The observed differences highlight the critical role of cellulose morphology in influencing charge storage behavior. The CC composite exhibits stable capacitance across voltages, likely due to uniform porosity and efficient ion transport, supporting a dominant double-layer mechanism [48].

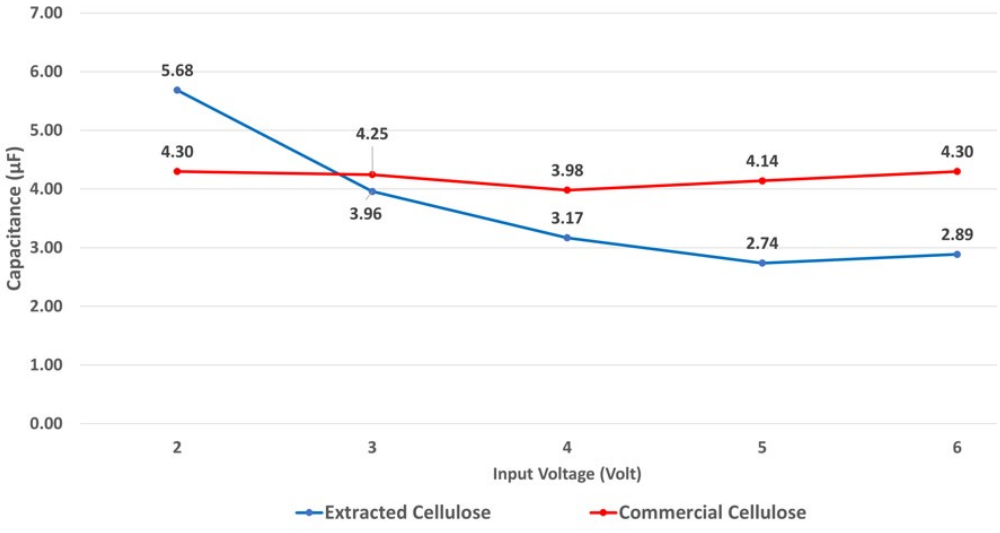

Fig. 6. Capacitance response of extracted and CC composites as a function of input voltage.

In contrast, the extracted cellulose composite shows voltage-dependent behavior, suggesting a stronger capacitive contribution [49]. Combining PPy with both cellulose types enhances conductivity and overall electrochemical performance, with the porous cellulose matrix aiding ion mobility and PPy providing redox activity [50, 51]. These results affirm the potential of PPy–cellulose composites as sustainable materials for advanced supercapacitor applications [52]. Building on our earlier work, which employed pineapple peel waste, the previous study successfully extracted micro-sized cellulose and identified a relationship between capacitance and voltage [53]. Although nanoscale cellulose had not yet been achieved, nor the correlation between current and voltage explored, the present findings are strengthened by the foundational insights gained in that prior research.

Figure 7 provides further insight into the electrochemical performance of both composites by illustrating their voltage (a)-(e) and current (f)-(j) profiles during charge–discharge cycles across the 2–6 V range. The PPy/Extracted Cellulose composite (blue) exhibits faster voltage transitions and higher current peaks, particularly at higher voltages, indicating enhanced charge-discharge responsiveness. This behavior suggests more efficient ion transport and lower internal resistance, which may be attributed to the extracted cellulose's finer structure or favorable surface chemistry. Meanwhile, the CC (red) exhibits a faster charging–discharging rate at an input voltage of 2 V. However, the rate gradually slows down as the voltage increases to 3, 4, 5, and 6 V. This voltage-dependent behavior is typical of capacitive materials, where redox-active sites become saturated or ion mobility is impeded at higher voltages due to increased internal resistance and polarization effects. This phenomenon highlights the critical role of material morphology and interfacial interactions in optimizing electrochemical performance, particularly in charge storage and release mechanisms [54]. This nuanced understanding of voltage response is crucial for tailoring PPy/cellulose composites for specific electrochemical applications, ensuring optimal performance under varying operating conditions.

The NC–PPy composite successfully combines NC's structural and ionic transport roles with the faradaic properties of PPy, offering a stable capacitive response at low to moderate voltages. While conductivity improves with increasing voltage, a decline in capacitance at higher potentials suggests material limitations under extended stress. Nonetheless, the system performs well in moderate operating ranges, making it suitable for eco-friendly capacitors. Pineapple crown waste adds value through sustainability, positioning the biopolymer as a promising support material rather than a primary charge-storing component.

Although cyclic voltammetry (CV) was not conducted in this study, galvanostatic charge–discharge (GCD) profiles were obtained and provide a reliable evaluation of the charge storage performance. The nearly linear and symmetric charge–discharge curves confirm capacitive behavior, in line with previous reports on biomass-derived composites that employed both CV and GCD analyses [41, 42].

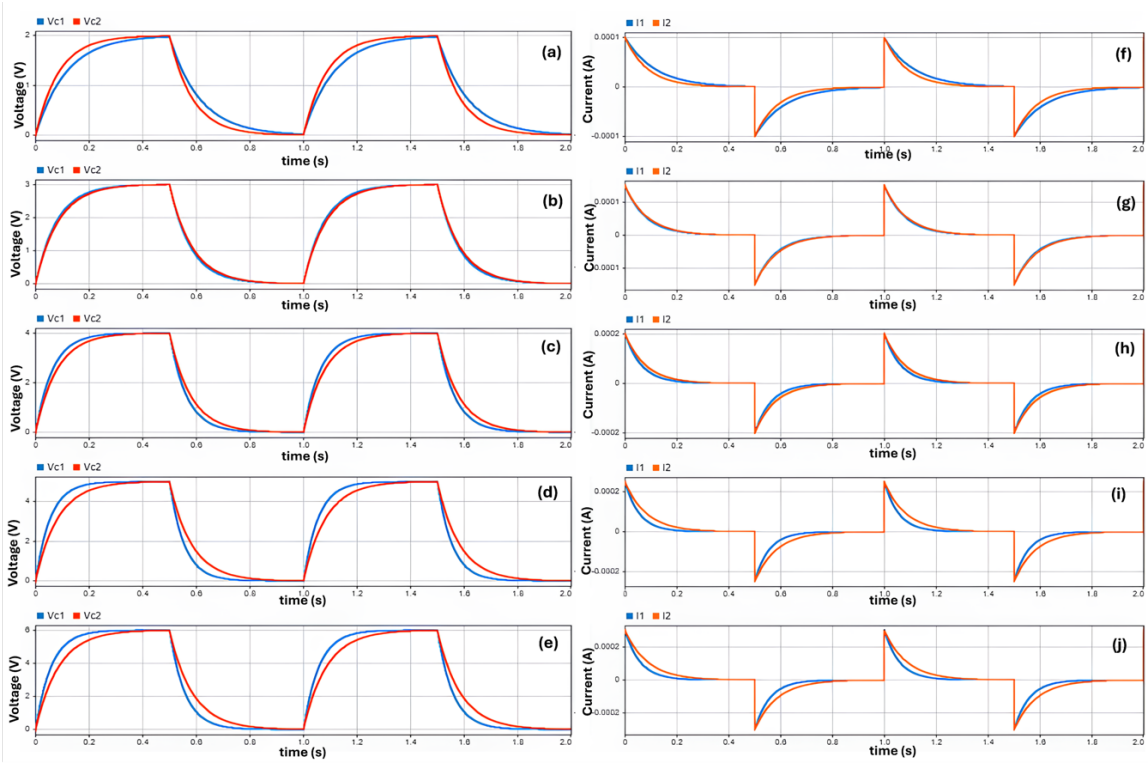

Fig.7. Charge–discharge voltage ((a)–(e)) and current ((f)–(j)) profiles of PPy composites with extracted cellulose (Vc1, blue; I1, blue) and CC (Vc2, red; I2, red) at applied voltages of 2–6 V. Input voltages: 2 V for (a) and (f); 3 V for (b) and (g); 4 V for (c) and (h); 5 V for (d) and (i); 6 V for (e) and (j). 4.

4. Conclusion

Hydrolysis at 50 °C was identified as the optimal condition for producing nanocellulose with favorable attributes, as indicated by sub-100 nm PSA and FT-IR evidence of lignin and hemicellulose removal. NC-50 also exhibited the highest crystallinity index based on XRD analysis. Using pineapple crown waste as a cellulose source adds value to agricultural residues and aligns with sustainable practices. Additionally, the resulting nanocellulose serves as an effective matrix in electrochemical systems, improving charge behavior at low voltages and showing promise for electrochemical applications requiring moderate voltage operation.

Availability of Data and Materials

The datasets used and analyzed during the current study are available from the corresponding author on reasonable request.

Author Contributions

BS and BP designed the research study. AA performed the cellulose extraction experiments, including delignification, bleaching, sulfuric acid hydrolysis, and ultrasonication. BP contributed to materials preparation, composite formulation, and structural characterization of the cellulose-based materials. BS drafted the manuscript. SDP provided conceptual guidance and contributed to data interpretation with emphasis on materials functionality and energy storage relevance. All authors contributed to critical revision of the manuscript for important intellectual content. All authors contributed to the critical revision of the manuscript for important intellectual content, read and

approved the final manuscript, participated sufficiently in the work, and agreed to be accountable for all aspects of the work.

Acknowledgement

The authors sincerely acknowledge the Mathematics and Natural Sciences Faculty, Universitas Tanjungpura, that supported this research through 2023 FMIPA DIPA grant.

Funding

This project was supported by the DIPA Research Grant from Faculty of Mathematics and Natural Sciences, Universitas Tanjungpura (Grant No.: 2689/UN22.8/PT.01.05/2023)

Conflict of Interest

The authors declare no conflict of interest.

References

[1] K. Deshmukh, M. B. Ahamed, R. R. Deshmukh, S. K. Pasha, P. R. Bhagat, K. Chidambaram, Elsevier, Amsterdam 27(2017). https://doi.org/10.1016/B978-0-12-809261-3.00003-6

[2] N. Muhd Julkapli, S. Bagheri, Polymers for Advanced Technologies **28**(12), 1583(2017). https://doi.org/10.1002/pat.4074

[3] K. Kupnik, M. Primožič, V. Kokol, M. Leitgeb, Polymers **12**(12), 2825(2020). https://doi.org/10.3390/polym12122825

[4] H. Gu, C. Gao, X. Zhou, A. Du, N. Naik, Z. Guo, Advanced Composites and Hybrid Materials **4**(3), 459(2021). https://doi.org/10.1007/s42114-021-00289-y

[5] K. Köse, M. Mavlan, J. P. Youngblood, Cellulose **27**(6), 2967(2020). https://doi.org/10.1007/s10570-020-03011-1

[6] N. Chanthathamrongsiri, A. Petchsomrit, N. Leelakanok, N. Siranonthana, T. Sirirak, Heliyon **7**(8), e07819(2021). https://doi.org/10.1016/j.heliyon.2021.e07819

[7] M. Zaki, H. P. S. A. K., F. A. Sabaruddin, R. D. Bairwan, A. A. Oyekanmi, T. Alfatah, M. Danish, E. M. Mistar, C. K. Abdullah, Bioresource Technology Reports **16**, 100811(2021). https://doi.org/10.1016/j.biteb.2021.100811

[8] M. Mahardika, H. Abral, A. Kasim, S. Arief, M. Asrofi, Fibers **6**(2), 28(2018). https://doi.org/10.3390/fib6020028

[9] D. Choquecahua Mamani, K. S. Otero Nole, E. E. Chaparro Montoya, D. A. Mayta Huiza, R.Y. Pastrana Alta, H. Aguilar Vitorino, Recycling **5**(4), 24(2020). https://doi.org/10.3390/recycling5040024

[10] K. S. Prado, M. A. Spinacé, International Journal of Biological Macromolecules **122**, 410(2019). https://doi.org/10.1016/j.ijbiomac.2018.10.187

[11] O. Nechyporchuk, M. N. Belgacem, J. Bras, Industrial Crops, Products **93**, 2(2016). https://doi.org/10.1016/j.indcrop.2016.01.004

[12] P. H. F. Pereira, H. L. Ornaghi Júnior, L. V. Coutinho, B. Duchemin, M. O. H. Cioffi, Cellulose **27**(10), 5745(2020). https://doi.org/10.1007/s10570-020-03179-6
[13] Y. Liu, A. Liu, S. A. Ibrahim, H. Yang, W. Huang, International Journal of Biological Macromolecules **111**, 717(2018). https://doi.org/10.1016/j.ijbiomac.2018.01.098
[14] L. Ravindran, M. S. Sreekala, S. Thomas, International Journal of Biological Macromolecules **131**, 858(2019). https://doi.org/10.1016/j.ijbiomac.2019.03.134
[15] S. L. Leong, S. I. X. Tiong, S. P. Siva, F. Ahamed, C. H. Chan, C. L. Lee, I. M. L. Chew, Y. K. Ho, Journal of Environmental Chemical Engineering **10**(4), 108145(2022). https://doi.org/10.1016/j.jece.2022.108145
[16] S. Jha, Y. Qin, Y. Chen, Z. Song, L. Miao, Y. Lv, L. Gan, M. Liu, Journal of Materials Chemistry A **13**(20), 15101(2025). https://doi.org/10.1039/d5ta00357a
[17] T. Shi, Z. Song, Y. Lv, D. Zhu, L. Miao, L. Gan, M. Liu, Chinese Chemical Letters **36**(1), 109559(2025). https://doi.org/10.1016/j.cclet.2024.109559
[18] N. Thinnakornsutibutr, T. Suracharoenchaikul, P. Potiyaraj, P. Pattananuwat, IOP Conference Series: Materials Science and Engineering **600**(1), 012007(2019). https://doi.org/10.1088/1757-899X/600/1/012007
[19] L. U. S. Faria, B. J. S. Pacheco, G. C. Oliveira, J. L. Silva, Journal of Materials Research and Technology **9**(6), 12346(2020). https://doi.org/10.1016/j.jmrt.2020.08.093
[20] M. Camacho, Y. R. C. Ureña, M. Lopretti, L. B. Carballo, G. Moreno, B. Alfaro, J. R. V. Baudrit, Journal of Renewable Materials **5**(3–4), 271(2017). https://doi.org/10.7569/JRM.2017.634117
[21] C. Trilokesh, K. B. Uppuluri, Scientific Reports **9**(1), 16709(2019). https://doi.org/10.1038/s41598-019-53412-x
[22] K. Rahbar Shamskar, H. Heidari, A. Rashidi, Journal of Polymers and the Environment **27**(7), 1418(2019). https://doi.org/10.1007/s10924-019-01438-7
[23] E. G. Bacha, South African Journal of Chemical Engineering **40**(1), 176(2022). https://doi.org/10.1016/j.sajce.2022.03.003
[24] S. B. Abd Hamid, S. K. Zain, R. Das, G. Centi, Carbohydrate Polymers **138**, 349(2016). https://doi.org/10.1016/j.carbpol.2015.10.023
[25] H. Holilah, H. Bahruji, R. Ediati, A. Asranudin, A. A. Jalil, B. Piluharto, R. E. Nugraha, D. Prasetyoko, International Journal of Biological Macromolecules **204**, 593(2022). https://doi.org/10.1016/j.ijbiomac.2022.02.045
[26] S. Mateo, S. Peinado, F. Morillas-Gutiérrez, M. D. La Rubia, A. J. Moya, Processes **9**(9), 1594(2021). https://doi.org/10.3390/pr9091594
[27] G. I. Bolio-López, R. E. Ross-Alcudia, L. Veleva, J. A. Azamar Barrios, G. C. M. Barrios, M. M. Hernández-Villegas, S. S. Córdova, Chem. Sci. Rev. Lett **5**(17), 198(2016).
[28] T. Theivasanthi, F. A. Christma, A. J. Toyin, S. C. Gopinath, R. Ravichandran, International Journal of Biological Macromolecules **109**, 832(2018). https://doi.org/10.1016/j.ijbiomac.2017.11.054
[29] N. S. Aprilia, N. Arahman, IOP Conference Series: Materials Science and Engineering **796**(1), 012007(2020). https://doi.org/10.1088/1757-899X/796/1/012012

[30] S. P. Espíndola, M. Pronk, J. Zlopasa, S. J. Picken, M. C. van Loosdrecht, Journal of Cleaner Production **280**, 124507(2021). https://doi.org/10.1016/j.jclepro.2020.124507
[31] M. Song, X. Hu, T. Gu, W. X. Zhang, Z. Deng, Journal of Environmental Chemical Engineering **10**(3), 107466(2022). https://doi.org/10.1016/j.jece.2022.107466
[32] J. H. Jordan, M. W. Easson, B. Dien, S. Thompson, B. D. Condon, Cellulose **26**(10), 5959(2019). https://doi.org/10.1007/s10570-019-02533-7
[33] L. T. Teixeira, W. F. Braz, R. N. C. de Siqueira, O. G. Pandoli, M. C. Geraldes, Journal of Materials Research and Technology **15**, 434 (2021). https://doi.org/10.1016/j.jmrt.2021.07.123
[34] M. A. Dar, R. Syed, K. D. Pawar, N. P. Dhole, R. Xie, R. S. Pandit, J. Sun, Environmental Technology & Innovation **27**, 102459(2022). https://doi.org/10.1016/j.eti.2022.102459
[35] K. C. C. de Carvalho Benini, H. J. C. Voorwald, M. O. H. Cioffi, M. C. Rezende, V. Arantes, Carbohydrate Polymers **192**, 337(2018). https://doi.org/10.1016/j.carbpol.2018.03.055
[36] R. A. Ilyas, S. M. Sapuan, M. R. Ishak, Carbohydrate Polymers **181**, 1038(2018). https://doi.org/10.1016/j.carbpol.2017.11.045
[37] I. Kouadri, H. Satha, Industrial Crops and Products **124**, 787(2018). https://doi.org/10.1016/j.indcrop.2018.08.051
[38] Y. Yang, J. Yang, J. Cao, Z. Wang, Bioresource Technology **267**, 517(2018). https://doi.org/10.1016/j.biortech.2018.07.038
[39] H. Abral, M. K. Chairani, M. D. Rizki, M. Mahardika, D. Handayani, E. Sugiarti, A. N. Muslimin, S. M. Sapuan, R. A. Ilyas, Journal of Materials Research and Technology **11**, 896(2021). https://doi.org/10.1016/j.jmrt.2021.01.057
[40] J. D. Hernández-Varela, J. J. Chanona Pérez, S. D. Gallegos-Cerda, H. A. Calderón Benavides, MRS Advances **6**(41), 941(2021). https://doi.org/10.1557/s43580-021-00139-5
[41] S. A. Fraser, W. E. van Zyl, RSC Advances **12**(34), 22031(2022). https://doi.org/10.1039/D2RA04320C
[42] C. Joel, S. D. Abraham, R. B. Bennie, M. S. M. Vasanth, B. Saravanakumar, S. Ansar, Y. A. Kumar, Journal of Power Sources **625**, 235649(2025). https://doi.org/10.1016/j.jpowsour.2024.235649
[43] W. J. Nicolas, D. Ghosal, E. I. Tocheva, E. M. Meyerowitz, G. J. Jensen, Journal of Bacteriology **203**(3), e00371-20(2021). https://doi.org/10.1128/jb.00371-20
[44] D. Y. Hastati, E. Hambali, K. Syamsu, E. Warsiki, Journal of the Japan Institute of Energy **98**(8), 194(2019). https://doi.org/10.3775/jie.98.194
[45] F. Scognamiglio, C. Santulli, G. Roselli, Curr. J. Appl. Sci. Technol **36**, 1(2019). https://doi.org/10.9734/CJAST/2019/v36i530254
[46] X. Lu, Z. Qiu, Y. Wan, Z. Hu, Y. Zhao, Composites Part A: Applied Science and Manufacturing **41**(10), 1516.(2010). https://doi.org/10.1016/j.compositesa.2010.06.014
[47] L. Zang, J. Qiu, E. Sakai, C. Yang, Advances in Polymer Technology **34**(3), 21497(2015). https://doi.org/10.1002/adv.21497
[48] H. M. Yadav, J. D. Park, H. C. Kang, J. Kim, J. J. Lee, Nanomaterials **11**(2), 395(2021). https://doi.org/10.3390/nano11020395

[49] M. Majumder, R. B. Choudhary, A. K. Thakur, Carbon **142**, 650(2019). https://doi.org/10.1016/j.carbon.2018.10.089
[50] M. Lian, X. Wu, Q. Wang, W. Zhang, Y. Wang, Ceramics International **43**(13), 9877(2017). https://doi.org/10.1016/j.ceramint.2017.04.171
[51] H. Liu, Q. Liu, H. You, L. Zang, M. Chen, C. Yang, Journal of Electroanalytical Chemistry **893**, 115332(2021). https://doi.org/10.1016/j.jelechem.2021.115332
[52] D. Shrestha, S. Maensiri, U. Wongpratat, S. W. Lee, A. R. Nyachhyon, Journal of Environmental Chemical Engineering **7**(5), 103227(2019). https://doi.org/10.1016/j.jece.2019.103227
[53] B. Sitorus, I. Syahbanu, F. Yoni, S. D. Panjaitan, Cellulose Chemistry & Technology **58**(3–4), 223(2024). https://doi.org/10.35812/CelluloseChemTechnol.2024.58.22
[54] J. Ma, D. Y. Su, Z. G. Liu, L. Jiang, J. Hao, Z. J. Zhang, X. K. Meng, IOP Conference Series: Earth and Environmental Science **267**(4), 042047(2019). https://doi.org/10.1088/1755-1315/267/4/042047